WEATHER CLIMATE WATER

WORLD METEOROLOGICAL ORGANIZATION

GLOBAL ATMOSPHERE WATCH

WMO GREENHOUSE GAS BULLETIN

The State of Greenhouse Gases in the Atmosphere Based on Global Observations through 2021

No. 18 | 26 October 2022

ISSN 2078-0796

In 2020 and 2021, the global network of the WMO Global Atmosphere Watch (GAW) Programme detected the largest within-year increases[1] (15 and 18 ppb,[2] respectively) of atmospheric methane (CH_4) since systematic measurements began in the early 1980s (Figure 1). The causes of these exceptional increases are still being investigated by the global greenhouse gas science community. Analyses of measurements of the abundances of atmospheric CH_4 and its stable carbon isotope ratio $^{13}C/^{12}C$ (reported as $\delta^{13}C(CH_4)$) (Figure 2) indicate that the increase in CH_4 since 2007 is associated with biogenic processes, but the relative contributions of anthropogenic and natural sources to this increase are unclear. While all conceivable efforts to reduce CH_4 emissions should be employed, this is not a substitute for reducing CO_2 emissions, whose impact on climate will continue for millennia.

Atmospheric CH_4 is the second largest contributor to climate change. Its effective direct radiative forcing (EDRF)[3] was 0.55 W m^{-2} in 2021 and over the past decade, it has been increasing by an average of 0.003 W m^{-2} yr^{-1}. In addition, because as CH_4 decays, it leads to the formation of tropospheric O_3 and stratospheric H_2O, in 2021, CH_4 led to an indirect radiative forcing of approximately 0.3 W m^{-2}. (For comparison, the EDRF from CO_2 was 2.22 W m^{-2} in 2021 and over the past decade, it has been increasing by an average of 0.03 W m^{-2} yr^{-1}.) The budget of CH_4 consists of a diverse mix of sources and sinks, with many sources overlapping spatially, so it is difficult to quantify emissions

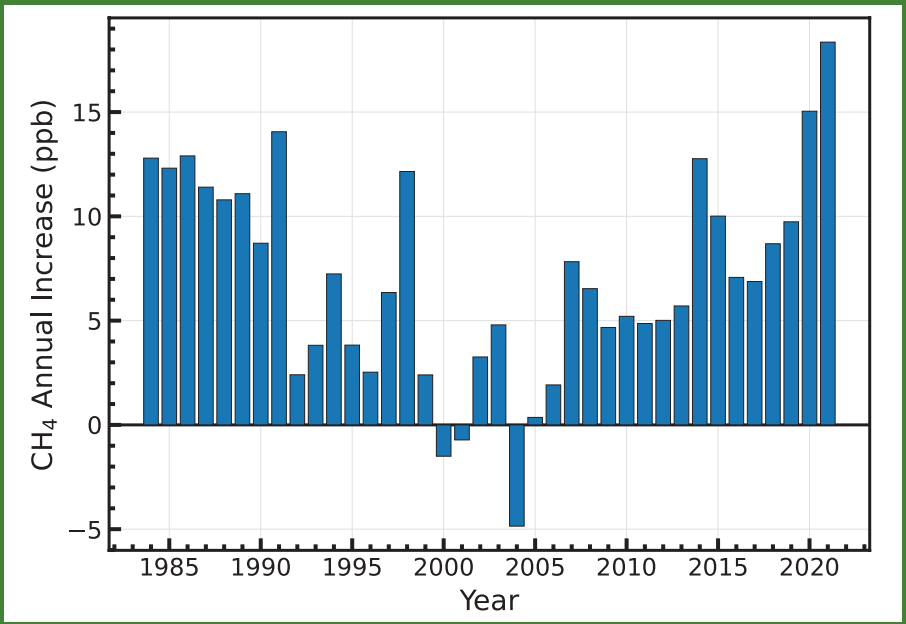

Figure 1. Within-year increases[1] of global average atmospheric CH_4 measured by the WMO GAW network over the period 1983–2021

by source type. Because of this, attributing changes in the growth rate of CH_4 to specific processes is a challenge. The best current constraints we have on the atmospheric CH_4 budget are from the long-term high-quality surface observations of CH_4 and $\delta^{13}C(CH_4)$ abundances by the WMO GAW community. These observations show conclusively that:

- Since 2007, globally averaged atmospheric CH_4 has been increasing;
- Its rate of increase is accelerating;
- The annual increases in 2020 and 2021 are the largest since the systematic record began in 1983.

Isotopic composition measurements show that globally averaged $\delta^{13}C(CH_4)$, after approximately 200 years of increase, started decreasing at nearly the same time as atmospheric CH_4 abundance began to increase again following a period of near-zero growth. While many scenarios of source and sink changes have been proposed to explain this renewed increase, which began in 2007, the most likely explanation, and one that is consistent with GAW CH_4 and $\delta^{13}C(CH_4)$ observations, is that it is due to increased emissions from predominantly biogenic sources. It is not yet possible to say if this is in part due to increased emissions from natural wetlands as a climate feedback. The record increases in 2020 and 2021 may also be attributable to interannual variability superimposed on a long-term increase in emissions. Understanding these changes remains an important matter for the scientific community.

There are cost-effective strategies available to mitigate anthropogenic CH_4 emissions, especially from the fossil fuel sector, which we know is a big source of CH_4 (greater than 20% of the total global emissions), and mitigating these emissions could have the added benefit of reducing CO_2 emissions. These strategies should be vigorously pursued. However, while the accumulation of methane in the atmosphere is reversible because of methane's relatively short lifetime (approximately 9 years), we must also take steps to reduce CO_2 emissions. The accumulation of CO_2 in the atmosphere is irreversible on human timescales and will affect climate for millennia by activating strong, slow feedbacks such as polar ice loss and sea-level rise.

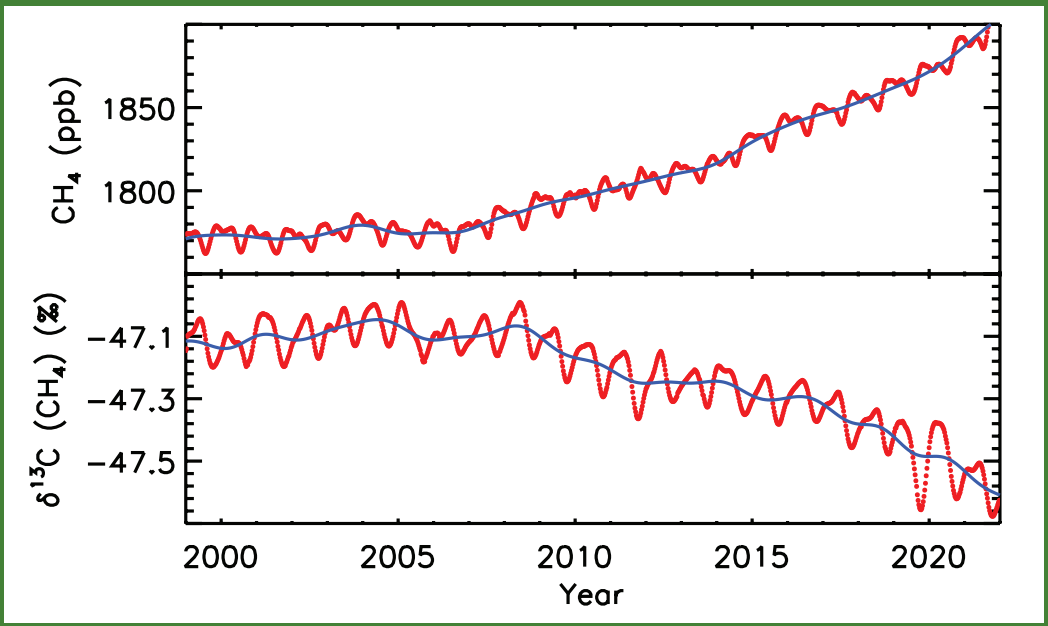

Figure 2. Smoothed (red lines) and deseasonalized (blue lines) global average atmospheric CH_4 and $\delta^{13}C(CH_4)$ measured by the global WMO GAW network

Executive summary

The latest analysis of observations from the WMO GAW in situ observational network shows that globally averaged surface mole fractions[4] for carbon dioxide (CO_2), methane (CH_4) and nitrous oxide (N_2O) reached new highs in 2021, with CO_2 at 415.7±0.2 ppm,[5] CH_4 at 1908±2 ppb and N_2O at 334.5±0.1 ppb. These values constitute, respectively, 149%, 262% and 124% of pre-industrial (before 1750) levels. The increase in CO_2 from 2020 to 2021 was equal to that observed from 2019 to 2020 and larger than the average annual growth rate over the last decade. For CH_4, the increase from 2020 to 2021 was higher than that observed from 2019 to 2020 and considerably higher than the average annual growth rate over the last decade. For N_2O, the increase from 2020 to 2021 was slightly higher than that observed from 2019 to 2020 and also higher than the average annual growth rate over the last decade. The National Oceanic and Atmospheric Administration (NOAA) Annual Greenhouse Gas Index (AGGI) [1] shows that from 1990 to 2021, radiative forcing by long-lived greenhouse gases (LLGHGs) increased by 49%, with CO_2 accounting for about 80% of this increase.

Overview of observations from the GAW in situ observational network for 2021

This eighteenth annual WMO Greenhouse Gas Bulletin reports atmospheric abundances and rates of change of the most important LLGHGs – carbon dioxide, methane and nitrous oxide – and provides a summary of the contributions of other greenhouse gases. CO_2, CH_4 and N_2O, together with dichlorodifluoromethane (CFC-12) and trichlorofluoromethane (CFC-11), account for approximately 96%[6] [1] of radiative forcing due to LLGHGs (Figure 3).

The WMO Global Atmosphere Watch Programme coordinates systematic observations and analyses of greenhouse gases (GHGs) and other trace species. Sites where GHGs have been measured in the last decade are shown in Figure 4. Measurement data are reported by participating countries and archived and distributed by the WMO World Data Centre for Greenhouse Gases (WDCGG) at the Japan Meteorological Agency.

The results reported here by WMO WDCGG for the global average and growth rate are slightly different from the results reported by NOAA for the same years (see [2] and the cover page of the present bulletin) due to differences in the stations used and the averaging procedure, as well as a slight difference in the time period for which the numbers are representative. WMO WDCGG follows the procedure described in detail in GAW Report No. 184 [3]. The results reported here for CO_2 differ slightly from those in the GHG bulletins issued before 2020 (by approximately 0.2 ppm) because data are now reported on the new WMO CO_2 X2019 calibration scale [4]. Historical data have been converted to the new scale to ensure consistency in reported trends.

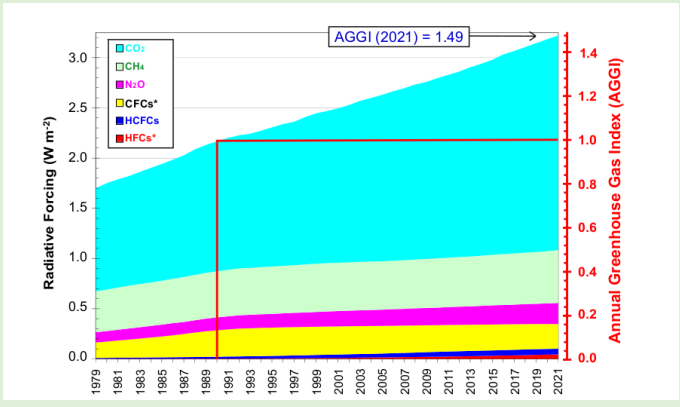

Figure 3. Atmospheric radiative forcing, relative to 1750, by LLGHGs, according to the 2021 update of the NOAA AGGI [1]

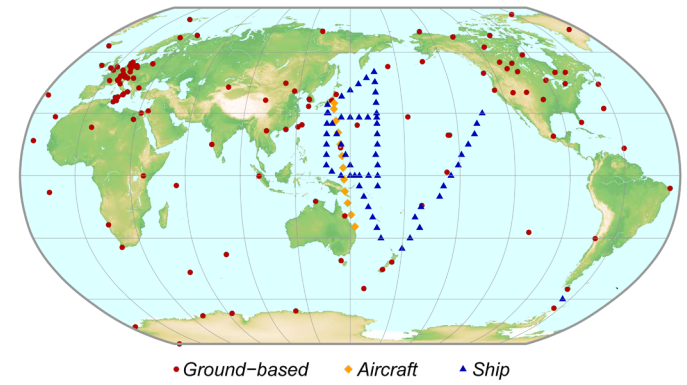

Figure 4. The GAW global network for carbon dioxide in the last decade. The network for methane is similar.

The table provides globally averaged atmospheric abundances of the three major LLGHGs in 2021 and changes in their abundances since 2020 and 1750. Data from mobile stations (blue triangles and orange diamonds in Figure 4), with the exception of data provided by NOAA sampling in the eastern Pacific, are not used for this global analysis.

The three GHGs shown in the table are closely linked to anthropogenic activities and interact strongly with the biosphere and the oceans. Predicting the evolution of the atmospheric content of GHGs requires a quantitative understanding of

Table. Global annual surface mean abundances (2021) and trends of key greenhouse gases from the GAW in situ observational network for GHGs. The units are dry-air mole fractions, and the uncertainties are 68% confidence limits. The averaging method is described in GAW Report No. 184 [3].

	CO_2	CH_4	N_2O
2021 global mean abundance	415.7±0.2 ppm	1908±2 ppb	334.5±0.1 ppb
2021 abundance relative to 1750[a]	149%	262%	124%
2020–21 absolute increase	2.5 ppm	18 ppb	1.3 ppb
2020–21 relative increase	0.61%	0.95%	0.39%
Mean annual absolute increase over the past 10 years	2.46 ppm yr^{-1}	9.2 ppb yr^{-1}	1.01 ppb yr^{-1}

[a] Assuming a pre-industrial mole fraction of 278.3 ppm for CO_2, 729.2 ppb for CH_4 and 270.1 ppb for N_2O. The number of stations used for the analyses was 147 for CO_2, 149 for CH_4 and 108 for N_2O.

(Continued on page 6)

An example of reducing future global warming: The Montreal Protocol and its Kigali Amendment

Guus Velders, Alex Vermeulen and Ray Weiss

The Montreal Protocol on Substances that Deplete the Ozone Layer, with its amendments and adjustments, regulates the production and consumption of a wide range of industrial ozone depleting substances (ODSs), mainly halocarbons, which catalyse the destruction of the Earth's protective stratospheric ozone layer. Adopted in 1987, the Protocol has been highly successful in reducing ODS emissions, in part because it is easier to regulate production and consumption than it is to regulate actual emissions. Beyond their impacts on ozone depletion, ODSs are also strong greenhouse gases, so their effective regulation to protect the ozone layer has also contributed more to reducing future global warming than any emission reduction in other greenhouse gases thus far.

Halocarbons that do not contain chlorine or bromine do not deplete stratospheric ozone, so in order to comply with the Montreal Protocol, many ODSs were initially replaced with hydrofluorocarbons (HFCs); however, HFCs are strong greenhouse gases. HFC emissions have increased dramatically over the past two decades, and in 2015, in the absence of regulations, large increases in HFC use and emissions were projected, potentially leading to up to 0.5 °C in additional global surface warming by 2100. In 2019, the Kigali Amendment to the Montreal Protocol came into force with the goal of limiting the use of HFCs globally. Currently, regulations to limit the use of HFCs are in effect in several countries (the United States of America ratified this amendment in September 2022).

According to the NOAA AGGI index, cited elsewhere in the present bulletin, halocarbons are currently responsible for 11% of the increased global radiative forcing that has occurred since 1750 (and thus for 0.13 °C of the current 1.3 °C global surface warming above 1750 levels). Without additional measures to control HFC consumption, an increased contribution to global average surface warming due to HFCs of 0.28–0.44 °C by 2100 has been estimated.

Due to a reduction in HFC emissions, recently detected by the AGAGE atmospheric monitoring network and other networks that contribute to the WMO GAW GHG global observations, this increase will be limited to between 0.14 and 0.31 °C by 2100. Following the additional controls of the Kigali Amendment, the reduction will be further limited to 0.04 °C. Although it is now difficult to achieve, a total ban on HFC consumption by 2023 would have contributed practically zero additional warming by 2100 [13]. This is further illustrated in Figure 10, which shows the projected additional warming due to halocarbons under the different assumptions for the period 2000–2100.

These are good examples of ways in which observations inform policymakers to take action to limit environmental damage and inform them of the progress being made to reach emission reduction targets. This, in turn, allows policymakers to further modify regulations to achieve the desired goals.

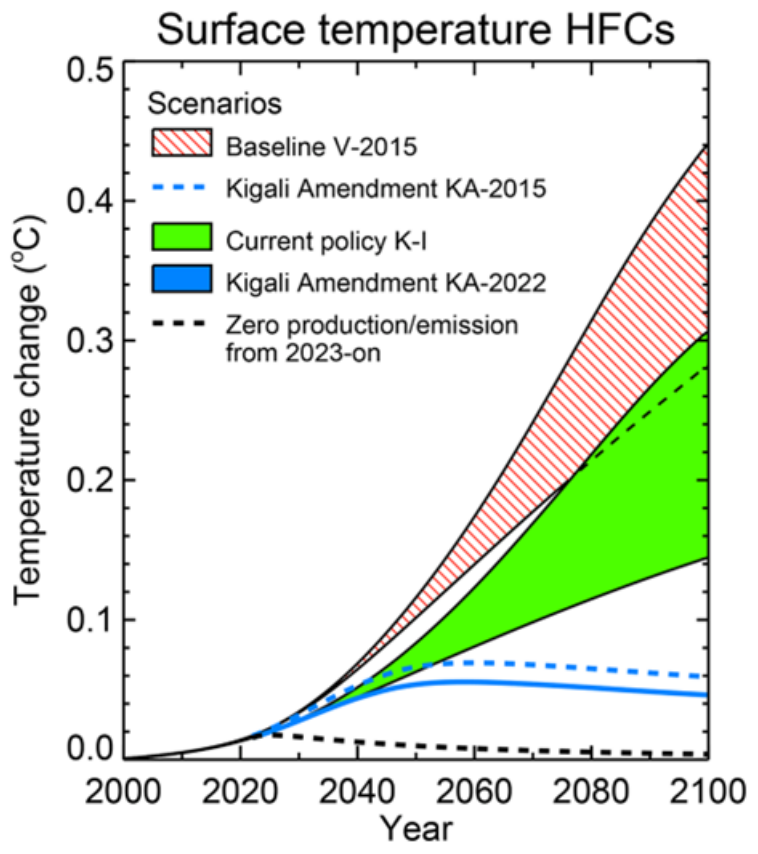

Figure 10. Contribution of HFCs to global average surface warming for the V-2015 baseline scenario without the implementation of measures affecting HFC consumption and the current policy of the Kigali-independent (K-I) scenario. The bands represent the upper and lower ranges of these scenarios. Also shown are the effects of the phasedown of HFCs following the controls of the Kigali Amendment (KA-2022) and a hypothetical scenario which assumes that the global production of HFC emissions will cease in 2023. No range is shown for the Kigali Amendment scenario since the lower and upper range scenarios virtually coincide. The surface temperature change is calculated using the MAGICC6 model. The curves contain the contributions of all HFCs except HFC-23 (see [13]).

The challenge of interpreting observed CH_4 growth rate variations

Sander Houweling and Ed Dlugokencky

The GAW greenhouse gas monitoring network accurately quantifies the global CH_4 growth rate, as noted in the cover story of the present bulletin. However, explaining the observed growth rate variations in terms of geographical origin and the main emission processes responsible is far more difficult. It requires untangling the dynamics of the atmosphere, which quickly disperses new emissions in large volumes of air before they reach the sampling points in the network. This is done using atmospheric tracer transport models. These models provide a detailed representation of the weather around the globe and compute its influence on the transport of gases. To estimate emissions from atmospheric measurements, the models compute the sensitivity of each measurement to each emission unit on a gridded map of surface emissions, which they monitor. A mathematical optimization procedure is used to find the emission configuration that enables the models to most closely agree with the measurements.

Computer codes using this so-called atmospheric inverse modelling method require supercomputers to be run at sufficient spatial and temporal resolutions. This is done, for example, by the European Copernicus Atmosphere Monitoring Service (CAMS), which has provided an annually updated reanalysis of measurement-derived emissions since 1990 [14]. Figure 11 shows how global CH_4 emissions have evolved over time, according to the latest CAMS reanalysis. Inverse modelling computations use inventories of emissions from fossil fuel use, agriculture, waste treatment, and so forth as a starting point, or a first guess. The difference between first guess (a priori) and inversion-optimized (a posteriori) emissions reflects the new information that the measurements provide.

The accuracy of emissions estimated from atmospheric measurements depends, in part, on the geometry of the surface network (see Figure 4 of the present bulletin). In regions with sparse observations, such as the tropical regions and the interior of the Asian continent, the estimated uncertainties of emissions are the largest. Most of the observed growth rate variations are nearly synchronous at different measurement sites around the Earth (see Figure 12), which inverse models translate into emission changes originating largely from the tropics. However, the limited availability of measurements in the tropical regions causes the uncertainties in the estimated emissions to remain high. The tropics accommodate not only highly uncertain emissions from natural wetlands, but also the atmospheric hydroxyl radical sink of CH_4, which is known to be largest there. Surface measurements provide limited information to distinguish between increasing surface emissions and reducing atmospheric sinks, which could both explain the increasing CH_4 abundance in the atmosphere. Methane-sensing satellites, such as GOSAT and TROPOMI, provide valuable additional coverage in the tropics; however, coverage remains poor over tropical forests because of the difficulty of satellites to detect methane in the presence of clouds. Expanding the in situ network in tropical regions with few stations, such as the tropical regions in Africa, will improve our knowledge of the source of CH_4 emissions considerably, as shown in a recent optimal network design study [15].

Measurements of stable isotopes provide powerful additional constraints on the origin of global trend fluctuations, as explained in the cover story of the present bulletin, strongly indicating a dominant role of microbial emissions in the recent CH_4 increase (see, for example, [16]). This, in combination with inversions pointing to a tropical origin, suggests that methane emissions from tropical wetlands might have increased in the past several years. Microbial methane production in tropical wetlands is sensitive to shifting temperature and precipitation patterns, introducing a potential positive climate feedback (this is a process which has received increasing scientific attention in studies conducted in recent years (see, for example, [17] and [18])). Methane emissions from tropical wetlands are also known to be sensitive to the El Niño Southern Oscillation (ENSO), as ENSO has an impact on temperature and precipitation patterns, and increased tropical methane emissions were reported by [19] during the strong La Niña of 2011. The La Niña phase that started in 2020 and is still ongoing might well have contributed to the recent record increases in the global growth rate of methane.

The main challenge of interpreting observed methane growth rate changes, however, is to prove which of several possible scenarios really happened. In the case of the 2020 growth rate increase, for example, the impact of COVID-19 lockdowns on atmospheric chemistry and the hydroxyl radical sink of methane may have been contributing factors [20]. However, atmospheric sinks are unlikely to explain the large annual CH_4 increase observed in 2021. The global methane budget initiative of the Global Carbon Project (GCP) plays an important role in synthesizing the information that is available from emission inventories, process-based models, and inverse models. The initiative uses an ensemble of models to assess model uncertainties. This is a process that takes several years, but at present, it is the only means of collecting enough information to determine the most likely explanation for the accelerating increase of atmospheric methane.

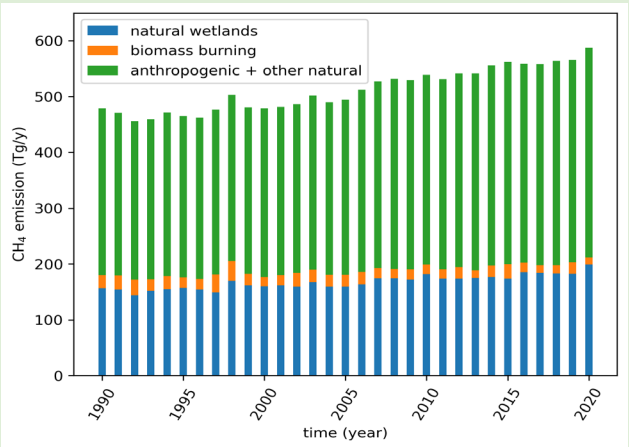

Figure 11. A posteriori CH_4 emissions from the CAMS inverse modelling reanalysis v20r1. The category "other natural" includes the uptake of methane by soils.

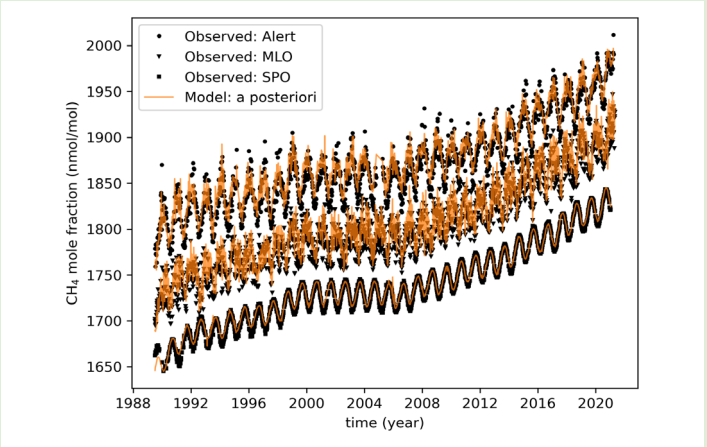

Figure 12. A posteriori fit of the CAMS CH_4 inverse model to selected station measurements (MLO = Mauna Loa station, SPO = South Pole station)

their many sources, sinks and chemical transformations in the atmosphere. Observations from GAW provide invaluable constraints on the budgets of these and other LLGHGs, and they are used to improve emission estimates and evaluate satellite retrievals of LLGHG column averages. The Integrated Global Greenhouse Gas Information System (IG^{3}IS) provides further insights on the sources of GHGs at the national and sub-national levels (https://ig3is.wmo.int).

Given the increasing focus on the role of GHGs as a driver of climate change and the need to strengthen the GHG information basis for decisions on climate mitigation efforts, WMO is working with the broader greenhouse gas community to develop a framework for sustained, internationally coordinated global greenhouse gas monitoring (see https://public.wmo.int/en/our-mandate/focus-areas/environment/greenhouse-gases/global-greenhouse-gas-monitoring-infrastructure). Pursuant to the decisions of the WMO Executive Council at its seventy-fifth session, a dedicated study group is currently developing the Greenhouse Gas Monitoring Infrastructure concept, which will establish an internationally coordinated approach to observing network design and to the acquisition, international exchange and use of the resulting observations. Within the framework of this infrastructure, WMO will engage and closely collaborate with both the broader scientific community and other United Nations agencies and international coordination entities involved in GHG monitoring activities, in particular with regard to land surface and ocean observation and modelling.

The NOAA AGGI measures the increase in total radiative forcing due to all LLGHGs since 1990 [1]. The AGGI reached 1.49 in 2021, representing a 49% increase in total radiative forcing[(6)] from 1990 to 2021 and a 1.2% increase from 2020 to 2021 (Figure 3). The total radiative forcing by all LLGHGs in 2021 (3.22 W m^{-2}) corresponds to an equivalent CO_2 mole fraction of 508 ppm [1]. The relative contributions of the major greenhouse gases to the total radiative forcing since the pre-industrial era are presented in Figure 5.

Carbon Dioxide (CO_2)

Carbon dioxide is the single most important anthropogenic greenhouse gas in the atmosphere, accounting for approximately 66%[(6)] of the radiative forcing by LLGHGs. It is responsible for about 81%[(6)] of the increase in radiative forcing over the past

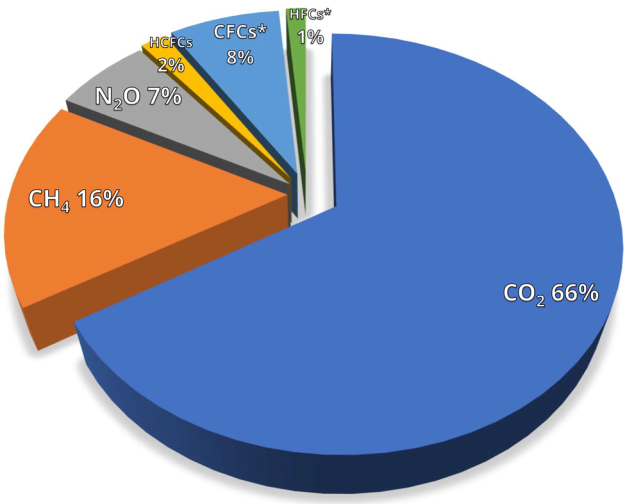

Figure 5. Contribution of the most important long-lived greenhouse gases to the increase in global radiative forcing from the pre-industrial era to 2021 [1]

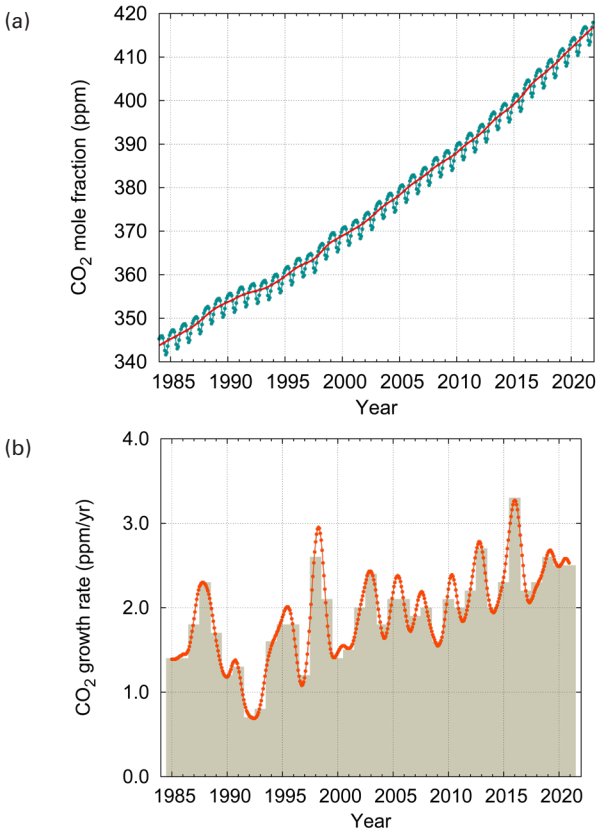

Figure 6. Globally averaged CO_2 mole fraction (a) and its growth rate (b) from 1984 to 2021. Increases in successive annual means are shown as the shaded columns in (b). The red line in (a) is the monthly mean with the seasonal variation removed; the blue dots and blue line in (a) depict the monthly averages. Observations from 147 stations were used for this analysis.

decade and about 80% of the increase over the past five years. The pre-industrial level of 278.3 ppm represented a balance of fluxes among the atmosphere, the oceans and the land biosphere. The globally averaged CO_2 mole fraction in 2021 was 415.7±0.2 ppm (Figure 6). The increase in the annual mean from 2020 to 2021, 2.5 ppm, was equal to the increase from 2019 to 2020 but slightly higher than the average growth rate for the past decade (2.46 ppm yr^{-1}).

Atmospheric CO_2 reached 149% of the pre-industrial level in 2021, primarily because of emissions from the combustion of fossil fuels and cement production. According to the International Energy Agency, global CO_2 emissions from energy combustion and industrial processes rebounded to 36.3 $GtCO_2$[(7)] in 2021, up 6% from 34.2 $GtCO_2$ in 2020, during which emissions were reduced with respect to the levels of the previous year due to COVID-19 restrictions [5, 6]. According to the 2021 analysis of the Global Carbon Project [7], deforestation and other land-use change contributed 4.1 (±2.6) $GtCO_2$ yr^{-1}, on average, for the 2011–2020 period. Of the total emissions from human activities during the 2011–2020 period, about 48% accumulated in the atmosphere, 26% in the ocean and 29% on land, with the unattributed budget imbalance being 3% [7]. The portion of CO_2 emitted by fossil fuel combustion that remains in the atmosphere (airborne fraction), varies inter-annually due to the high natural variability of CO_2 sinks without a confirmed global trend (see also the cover story in WMO Greenhouse Gas Bulletin No. 17).

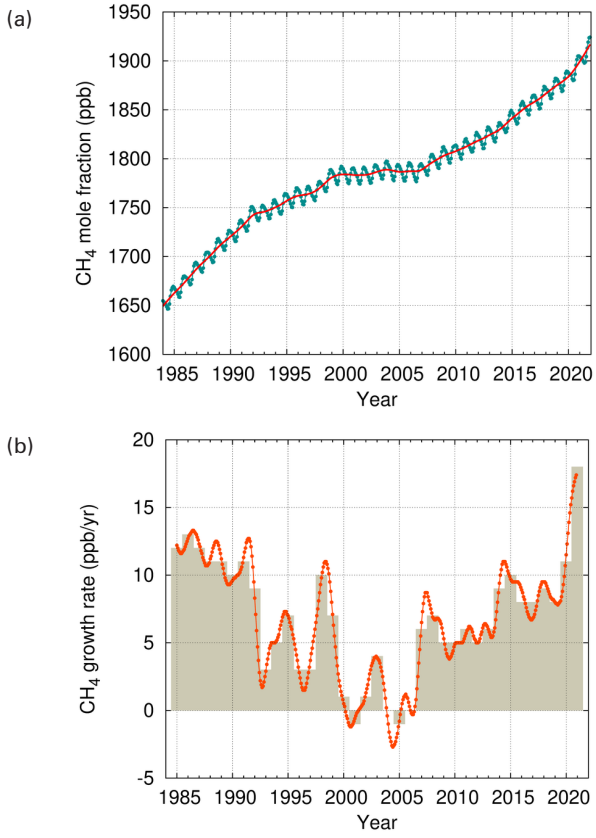

Figure 7. Globally averaged CH_4 mole fraction (a) and its growth rate (b) from 1984 to 2021. Increases in successive annual means are shown as the shaded columns in (b). The red line in (a) is the monthly mean with the seasonal variation removed; the blue dots and blue line in (a) depict the monthly averages. Observations from 149 stations were used for this analysis.

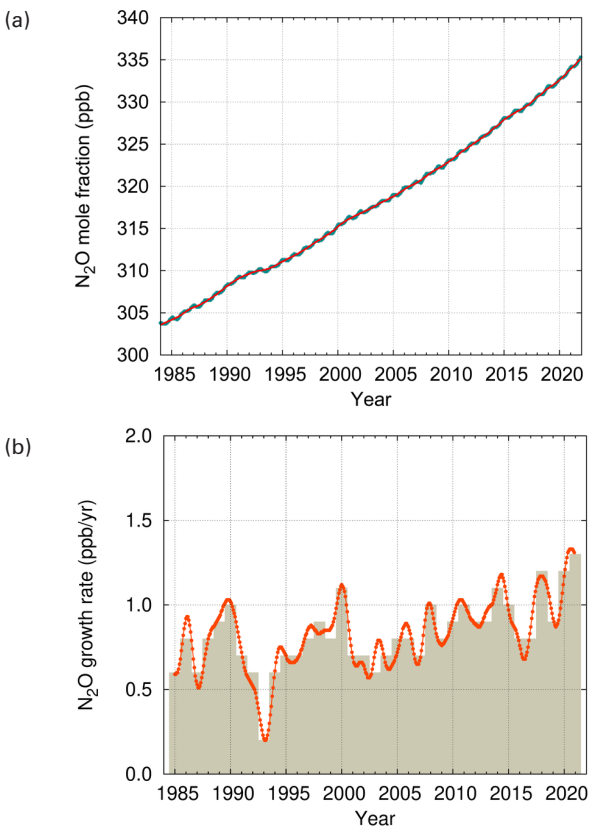

Figure 8. Globally averaged N_2O mole fraction (a) and its growth rate (b) from 1984 to 2021. Increases in successive annual means are shown as the shaded columns in (b). The red line in (a) is the monthly mean with the seasonal variation removed; in this plot, the red line overlaps the blue dots and blue line that depict the monthly averages. Observations from 108 stations were used for this analysis.

Methane (CH_4)

Methane accounts for about 16%[6] of the radiative forcing by LLGHGs. Approximately 40% of methane is emitted into the atmosphere by natural sources (for example, wetlands and termites), and about 60% comes from anthropogenic sources (for example, ruminants, rice agriculture, fossil fuel exploitation, landfills and biomass burning) [8]. The globally averaged CH_4 mole fraction calculated from in situ observations reached a new high of 1908 ± 2 ppb in 2021, an increase of 18 ppb with respect to the previous year (Figure 7). This increase is higher than the increase of 11 ppb from 2019 to 2020 and higher than the average annual increase over the past decade. The mean annual increase of CH_4 decreased from approximately 12 ppb yr^{-1} during the late 1980s to near zero during 1999–2006. Since 2007, atmospheric CH_4 has been increasing, reaching 262% of the pre-industrial level due to increased emissions from anthropogenic sources. Studies using GAW CH_4 measurements indicate that increased CH_4 emissions from wetlands in the tropics and from anthropogenic sources at the mid-latitudes of the northern hemisphere are the likely causes of this recent increase. More details on the increase in atmospheric CH_4 can be found in the cover story and the insert of the present bulletin.

Nitrous Oxide (N_2O)

Nitrous oxide accounts for about 7%[6] of the radiative forcing by LLGHGs. It is the third most important individual contributor to the combined forcing. N_2O is emitted into the atmosphere from both natural sources (approximately 57%) and anthropogenic sources (approximately 43%), including oceans, soils, biomass burning, fertilizer use, and various industrial processes [9]. The globally averaged N_2O mole fraction in 2021 reached 334.5 ±0.1 ppb, which is an increase of 1.3 ppb with respect to the previous year (Figure 8) and 124% of the pre-industrial level (270.1 ppb). The annual increase from 2020 to 2021 was higher than the increase from 2019 to 2020 and also higher than the mean growth rate over the past 10 years (1.01 ppb yr^{-1}). Global human-induced N_2O emissions, which are dominated by nitrogen additions to croplands, increased by 30% over the past four decades to 7.3 (range: 4.2–11.4) teragrams of nitrogen per year. This increase was mainly responsible for the growth in the atmospheric burden of N_2O [9].

Other greenhouse gases

Stratospheric ozone-depleting chlorofluorocarbons (CFCs), which are regulated by the Montreal Protocol on Substances that Deplete the Ozone Layer, together with minor halogenated gases, account for approximately 11%[6] of the radiative forcing by LLGHGs. While CFCs and most halons are decreasing, some hydrochlorofluorocarbons (HCFCs) and hydrofluorocarbons (HFCs), which are also potent greenhouse gases, are increasing at relatively rapid rates; however, they are still low in abundance (at ppt[8] levels). Although at a similarly low abundance, sulfur hexafluoride (SF_6) is an extremely potent LLGHG. It is produced by the chemical industry, mainly as an electrical insulator in power distribution equipment. Its current mole fraction is more than twice the level observed in the mid-1990s (Figure 9(a)).

The present bulletin primarily addresses long-lived greenhouse gases. Relatively short-lived tropospheric ozone has a radiative

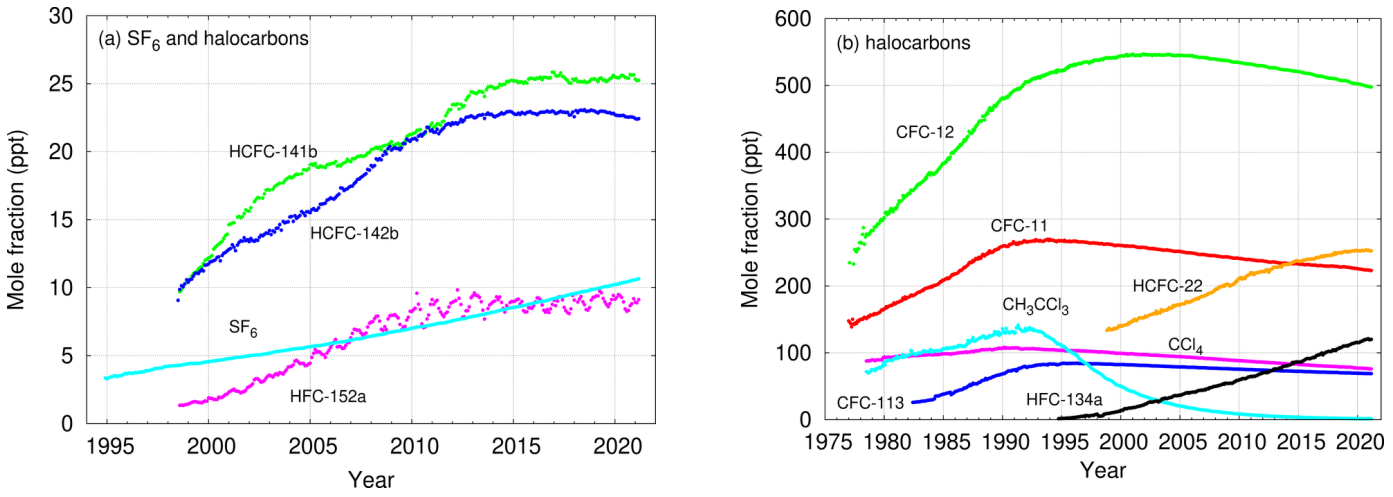

Figure 9. Monthly mean mole fractions of sulfur hexafluoride (SF_6) and the most important halocarbons: (a) SF_6 and lower halocarbon mole fractions and (b) higher halocarbon mole fractions. For each gas, the number of stations used for the analysis was as follows: SF_6 (88), CFC-11 (23), CFC-12 (25), CFC-113 (22), CCl_4 (22), CH_3CCl_3 (25), HCFC-141b (11), HCFC-142b (15), HCFC-22 (14), HFC-134a (12), HFC-152a (11).

forcing comparable to that of the halocarbons [10]. Many other pollutants, such as carbon monoxide, nitrogen oxides and volatile organic compounds, although not referred to as greenhouse gases, have small direct or indirect effects on radiative forcing. Aerosols (suspended particulate matter) are short-lived substances that alter the radiation budget. All the gases mentioned in the present bulletin, as well as aerosols, are included in the observational programme of GAW, with support from WMO Member countries and contributing networks [11].

Acknowledgements and links

Fifty-five WMO Members contributed CO_2 and other greenhouse gas data to the GAW WDCGG. Approximately 39% of the measurement records submitted to WDCGG were obtained at sites of the NOAA Global Monitoring Research Laboratory cooperative air-sampling network. For other networks and stations, see [12]. The Advanced Global Atmospheric Gases Experiment also contributed observations to the present bulletin. The GAW observational stations that contributed data to the present bulletin, shown in Figure 4, are included in the list of contributors on the WDCGG web page. They are also described in the GAW Station Information System (GAWSIS), supported by the Swiss Federal Office for Meteorology and Climatology (MeteoSwiss). The present bulletin has been prepared under the oversight of the GAW Scientific Advisory Group on Greenhouse Gases.

Editorial team

Alex Vermeulen (Integrated Carbon Observation System – European Research Infrastructure Consortium (ICOS ERIC)/ Lund University, Sweden), Yousuke Sawa (Japan Meteorological Agency, WDCGG, Japan), Oksana Tarasova (WMO)

Authors (in alphabetical order)

Andy Crotwell (NOAA Global Monitoring Laboratory and Cooperative Institute for Research in Environmental Sciences, University of Colorado Boulder, United States of America), Ed Dlugokencky (NOAA Global Monitoring Laboratory), Christoph Gerbig (Max Planck Institute for Biogeochemistry, Germany), David Griffith (University of Wollongong, Australia), Bradley Hall (NOAA Global Monitoring Laboratory, United States of America), Sander Houweling (Vrije Universiteit, Amsterdam, The Netherlands), Armin Jordan (Max Planck Institute for Biogeochemistry, Germany), Paul Krummel (Commonwealth Scientific and Industrial Research Organisation, Australia), Haeyoung Lee (Korea Meteorological Administration, National Institute of Meteorological Sciences, Republic of Korea), Zoë Loh (Commonwealth Scientific and Industrial Research Organisation, Australia), Yousuke Sawa (Japan Meteorological Agency, WDCGG, Japan), Oksana Tarasova (WMO), Jocelyn Turnbull (GNS Science, New Zealand/Cooperative Institute for Research in Environmental Sciences, University of Colorado Boulder, United States of America), Guus Velders (National Institute for Public Health and the Environment, Bilthoven, Netherlands), Alex Vermeulen (ICOS ERIC/Lund University, Sweden), Ray Weiss (Scripps Institute of Oceanography, University of California San Diego, United States of America)

References

[1] Montzka, S. A. T*he NOAA Annual Greenhouse Gas Index (AGGI). National Oceanic and Atmospheric Administration (NOAA)* Earth System Research Laboratories Global Monitoring Laboratory, 2022. http://www.esrl.noaa.gov/gmd/aggi/aggi.html.

[2] National Oceanic and Atmospheric Administration (NOAA) Earth System Research Laboratories Global Monitoring Laboratory. *Trends in Atmospheric Carbon Dioxide*, 2022. http://www.esrl.noaa.gov/gmd/ccgg/trends/.

[3] Tsutsumi, Y.; Mori, K.; Hirahara, T. et al. *Technical Report of Global Analysis Method for Major Greenhouse Gases by the World Data Center for Greenhouse Gases* (WMO/TD-No. 1473). GAW Report No. 184. World Meteorological Organization (WMO): Geneva, 2009.

[4] Hall, B. D.; Crotwell, A. M.; Kitzis, D. R. et al. Revision of the World Meteorological Organization Global Atmosphere Watch (WMO/GAW) CO_2 Calibration Scale. *Atmospheric Measurement Techniques* **2021**, *14* (4), 3015–3032. https://doi.org/10.5194/amt-14-3015-2021.

[5] Le Quéré, C.; Jackson, R. B.; Jones, M. W. et al. Temporary Reduction in Daily Global CO_2 Emissions during the COVID-19 Forced Confinement. *Nat. Clim. Chang.* **2020**, *10* (7), 647–653. https://doi.org/10.1038/s41558-020-0797-x.

[6] International Energy Agency (IEA). *Global Energy Review: CO2 Emissions in 2021*; IEA: Paris, 2022. https://www.iea.org/reports/global-energy-review-co2-emissions-in-2021-2.

[7] Friedlingstein, P.; Jones, M. W.; O'Sullivan, M. et al. Global Carbon Budget 2021. *Earth System Science Data* **2022**, *14* (4), 1917–2005. https://doi.org/10.5194/essd-14-1917-2022.

[8] Saunois, M.; Stavert, A. R.; Poulter; B. et al., The Global Methane Budget 2000–2017. *Earth System Science Data* **2020**, *12* (3), 1561–1623. https://doi.org/10.5194/essd-12-1561-2020.

[9] Tian, H.; Xu, R.; Canadell, J. G. et al. A Comprehensive Quantification of Global Nitrous Oxide Sources and Sinks. *Nature* **2020**, *586* (7828), 248–256. https://doi.org/10.1038/s41586-020-2780-0.

[10] World Meteorological Organization (WMO). *WMO Reactive Gases Bulletin: Highlights from the Global Atmosphere Watch Programme, No. 2*; WMO: Geneva, 2018.

[11] World Meteorological Organization (WMO). *WMO Air Quality and Climate Bulletin, No. 2*; WMO: Geneva, 2022.

[12] World Meteorological Organization (WMO). *20th WMO/IAEA Meeting on Carbon Dioxide, Other Greenhouse Gases and Related Measurement Techniques (GGMT-2019)*. GAW Report No. 255; WMO: Geneva, 2020.

[13] Velders, G. J. M.; Daniel, J. S.; Montzka, S. A. et al. Projections of Hydrofluorocarbon (HFC) Emissions and the Resulting Global Warming Based on Recent Trends in Observed Abundances and Current Policies. *Atmospheric Chemistry and Physics* **2022**, *22* (9), 6087–6101, https://doi.org/10.5194/acp-22-6087-2022.

[14] Segers, A. J.; Tokaya, J.; Houweling, S. *Description of the CH4 Inversion Production Chain*; Copernicus Atmosphere Monitoring Service, 2020. https://atmosphere.copernicus.eu/sites/default/files/2021-01/CAMS73_2018SC3_D73.5.2.2-2020_202012_production_chain_Ver1.pdf.

[15] Nickless, A.; Scholes, R. J.; Vermeulen, A. et al. Greenhouse Gas Observation Network Design for Africa. Tellus B: *Chemical and Physical Meteorology* **2020**, *72* (1), 1824486. https://doi.org/10.1080/16000889.2020.1824486.

[16] Lan, X.; Basu, S.; Schwietzke, S. et al. Improved Constraints on Global Methane Emissions and Sinks Using δ13C-CH4. *Global Biogeochemical Cycles* **2021**, *35* (6), e2021GB007000. https://doi.org/10.1029/2021GB007000.

[17] Lunt, M. F.; Palmer, P. I.; Feng, L. et al. An Increase in Methane Emissions from Tropical Africa between 2010 and 2016 Inferred from Satellite Data. *Atmospheric Chemistry and Physics* **2019**, *19* (23), 14721–14740. https://doi.org/10.5194/acp-19-14721-2019.

[18] Feng, L.; Palmer, P. I.; Zhu, S. et al. Tropical Methane Emissions Explain Large Fraction of Recent Changes in Global Atmospheric Methane Growth Rate. *Nature Communications* **2022**, *13* (1), 1378. https://doi.org/10.1038/s41467-022-28989-z.

[19] Pandey, S.; Houweling, S.; Krol, M. et al. Enhanced Methane Emissions from Tropical Wetlands during the 2011 La Niña. *Scientific Reports* **2017**, *7* (1), 45759. https://doi.org/10.1038/srep45759.

[20] Gkatzelis, G. I.; Gilman, J. B.; Brown, S. S. et al. The Global Impacts of COVID-19 Lockdowns on Urban Air Pollution: A Critical Review and Recommendations. *Elementa: Science of the Anthropocene* **2021**, *9* (1), 00176. https://doi.org/10.1525/elementa.2021.00176.

Contacts

World Meteorological Organization
Atmospheric Environment Research Division, Science and Innovation Department, Geneva
Email: gaw@wmo.int
Website: https://community.wmo.int/activity-areas/gaw

World Data Centre for Greenhouse Gases
Japan Meteorological Agency, Tokyo
Email: wdcgg@met.kishou.go.jp
Website: https://gaw.kishou.go.jp

Notes:

(1) Within-year increases of atmospheric CH_4 are calculated as the increase in atmospheric CH_4 on a deseasonalized trend line from 1 January of one year to 1 January of the following year, in accordance with the data reported on the National Oceanic and Atmospheric Administration (NOAA) Trends in CH_4 web page.

(2) ppb = The number of molecules of a gas per billion (10^9) molecules of dry air

(3) Radiative forcing is the perturbation to the Earth's energy budget resulting from the increased burdens of greenhouse gases since the pre-industrial (1750) period after allowing stratospheric temperature to quickly adjust. "Effective" radiative forcing also includes fast tropospheric adjustments. Note that the numbers presented here account only for the direct radiative forcing of CH_4 and CO_2, as opposed to the emission-based forcings used in the IPCC AR6 WG1 report, which include estimated indirect forcings due to the atmospheric chemistry of CH_4, influencing other atmospheric constituents.

(4) Mole fraction = The preferred expression for the abundance (concentration) of a mixture of gases or fluids. In atmospheric chemistry, the mole fraction is used to express the concentration as the number of moles of a compound per mole of dry air.

(5) ppm = The number of molecules of a gas per million (10^6) molecules of dry air

(6) This percentage is calculated as the relative contribution of the mentioned gas(es) to the increase in global radiative forcing caused by all long-lived greenhouse gases since 1750.

(7) 1 $GtCO_2$ = 1 billion (10^9) metric tons of carbon dioxide

(8) ppt = The number of molecules of a gas per trillion (10^{12}) molecules of dry air

Selected greenhouse gas observatories

Sodankylä/Pallas (SDK/PAL)

Sodankylä station

The Sodankylä/Pallas site consists of the Arctic Space Centre in Sodankylä and a clean air research station in Pallas. The distance between these two sites is 125 km. They are both hosted and owned by Finnish Meteorological Institute.

The Sodankylä station (SDK) was established in 1949, but there are records of continuous homogenized synoptic weather data from 1908 onwards from the site. The facility is now 1500 m^2 and includes multiple buildings, as well as supporting masts in a forest and swamp field and multiple aerial measurement camps.

The observatory forms the upper atmosphere part of the Finnish GAW site and provides vertically resolved meteorological and ozone data and data on particles in the stratosphere. The observatory is located in central Lapland, north of the Arctic Circle. Sodankylä is a GAW Global Station and part of the Network for the Detection of Atmospheric Composition Change, the Total Carbon Column Observing Network and the Aerosol Robotic Network, which are remote sensing networks.

Pallas station

Pallas (PAL) has been operating since 1994. It is a GAW Global Station for greenhouse gases and part of the Integrated Carbon Observation System (ICOS), the Aerosol, Cloud and Trace Gases Research Infrastructure (ACTRIS) and the Integrated European Long-Term Ecosystem, Critical Zone and Socio-Ecological Research (eLTER) networks.

Location
Country: Finland
Latitude: 67.364°N
Longitude: 26.63°E
Elevation: 180 m asl
Time zone: UTC +2

Jeju Gosan GAW Regional Observatory (GSN)

Gosan GAW station

The Gosan GAW station on Jeju Island of South Korea is situated in the northern part of the East China Sea, about 100 km south of the Korean peninsula, 500 km north-east of Shanghai, China, and 250 km west of Kyushu, Japan. The Gosan site is located at the western edge of the island at the top of a 72 m cliff, facing the East China Sea. Jeju Island is regarded as one of the cleanest areas in South Korea. This station monitors more than 22 GAW atmospheric constituents, including greenhouse gases, aerosols, and reactive gases. Since the 1990s, it has been used for international campaigns such as Aerosol Characterization Experiment (ACE)-Asia and the Atmospheric Brown Cloud campaign, as well as for the Advanced Global Atmospheric Gases Experiment (AGAGE). It has also been part of the Asian Dust and Aerosol Lidar Observation Network (ADNet) and other international networks in addition to being part of the GAW network of stations.

Location
Country: Republic of Korea
Latitude: 33.294°N
Longitude: 126.163°E
Elevation: 71 m asl
Time zone: UTC +9

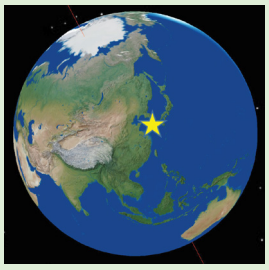

JN 22988